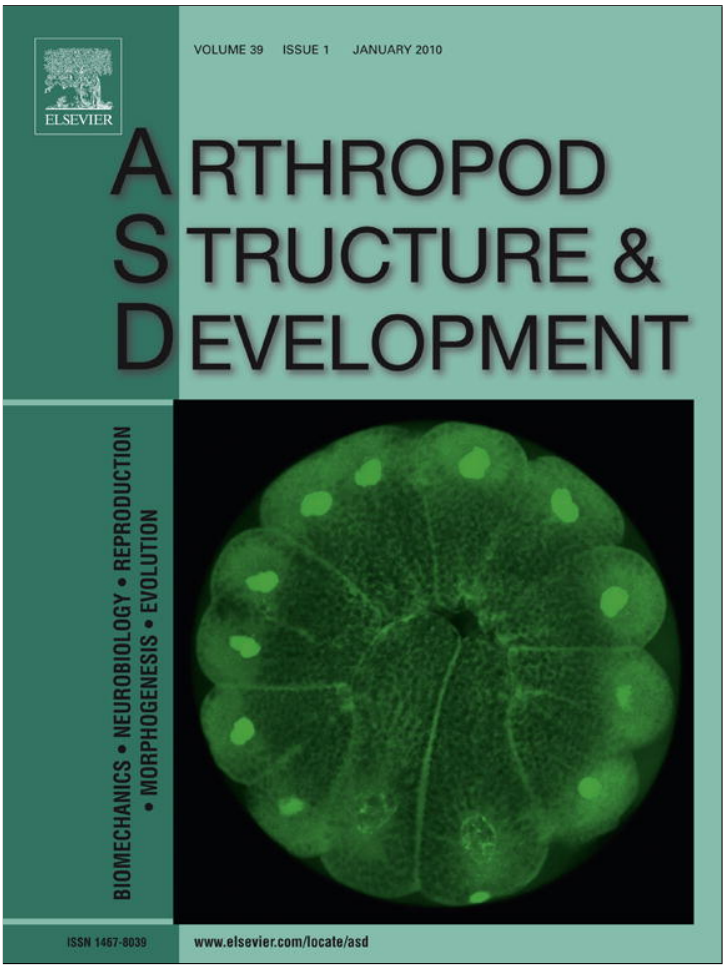

Arthropod Structure & Development 39 (2010) 1–16

Contents lists available at ScienceDirect

Arthropod Structure & Development

journal homepage: www.elsevier.com/locate/asd

Moth olfactory trichoid sensilla exhibit nanoscale-level heterogeneity in surface lipid properties

Masato M. Maitani [a], David L. Allara [a,b], Kye Chung Park [c,1], Seong Gyu Lee [c,2], Thomas C. Baker [c,*]

[a] Department of Materials Science and Engineering, Penn State University, University Park, PA 16802, USA
[b] Department of Chemistry, Penn State University, University Park, PA 16802, USA
[c] Center for Chemical Ecology and Department of Entomology, Penn State University, University Park, PA 16802, USA

ARTICLE INFO

Article history:
Received 6 July 2009
Accepted 17 August 2009

Keywords:
Insect
Sex pheromone
Olfaction
Sensillum
Cuticular lipids
Atomic force microscopy
Chemical force microscopy
Helicoverpa zea
Utethesia ornatrix

ABSTRACT

Chemical force microscopy (CFM) based on tapping mode Atomic force microscopy (AFM) utilized with topographic and phase-shift analyses was used to investigate the topography and surface chemical properties, respectively, of the long trichoid sensilla on the antennae of male *Helicoverpa zea*. AFM topographic imaging revealed regular series of step-ridges along nearly the entire length of each sensillum, except for the basal ca. 1/3 portions, which were devoid of such ridges. Inter-ridge regions were flat, with regularly spaced pores, ca. 30 nm in diameter populating these planar areas. Many pores exhibited a raised dome that often nearly completely spanned the depression, with only the edges of the depressed portion of the pore still visible. Some pores were observed also along the bases of the ridges. CFM probing of the surface for chemical interactions with the SiO_2 hydrophilic tip revealed consistently diminished hydrogen bonding of the ridge edge areas with the tip than along the flat planar inter-ridge regions. Surfaces of domes over the pores also tended to have less hydrogen bonding with the tip than the planar surfaces. Functionalizing the CFM tip by bonding octadecyl-hydrocarbon to it eliminated these surface chemical-CFM tip interactions and no differences in tip interaction with the sensillar surfaces were observed. Trichoid sensilla from the male antennae of a second species, *Utethesia ornatrix*, did not exhibit similar heterogeneity between ridge edges versus planar areas with regard to hydrogen bonding with the SiO_2 hydrophilic tip. Pores on *U. ornatrix* sensilla occurred only along the bases of ridges on their trichoid sensilla. We suggest that the surface lipids of the *H. zea* sensilla are distributed in a chemically heterogeneous fashion to aid adsorption and transport of aldehyde pheromone component molecules through the pores into the sensillum lumen, possibly through solubilization in an epicuticular lipid layer. The trichoid sensilla of *U. ornatrix* do not exhibit such surface chemical heterogeneity, and this species-difference may be due to the usage by *U. ornatrix* of hydrocarbon molecules rather than aldehydes for their sex pheromone components.

1. Introduction

The functional unit on the antennae of male moths for adsorbing sex pheromone molecules from a pheromone plume is the organule (Lawrence, 1966) called a *sensillum trichodeum*. There are many tens of thousands of these trichoid sensilla on each of the paired antennae of male moths. Depending on the species, each such hair-like sensillum can range between ca. 10–400 μm in length and from 1 to 5 μm in diameter (Kaissling, 2004). Inside are the dendrites of two to three of the reporting units, the olfactory receptor neurons (ORNs), all of which send their axons to the brain to report their levels of excitation in response to components of the sex pheromone components to which they are specifically tuned.

When a pheromone component molecule contacts a sensillum, it must adsorb onto the exterior surface that is coated, like all the surfaces of insect cuticle, with complex mixtures of lipids, and then pass through a pore with its associated pore tubules into the sensillum lumen (Steinbrecht, 1987, 1997, 1999). The basic process by which odorant molecules are acquired from 3D space through adsorption onto a planar 2D surface and then undergoing a change from 2D to 1D diffusion into and down a pore and its pore tubules was brought to light by Adam and Delbruck (1968). Much research was devoted in the 1970s through the early 1990s to understanding the processes by which initial uptake of lipophilic odorant molecules occurs on sensilla, as well as to understanding the barriers

* Corresponding author. Tel.: +1 814 863 4435; fax: +1 814 863 4439.
E-mail address: tcb10@psu.edu (T.C. Baker).
[1] Present address: Plant and Food Research, Lincoln 8152, New Zealand.
[2] Present address: Department of Biology, University of Utah, Salt Lake City, UT, USA.

1467-8039/$ – see front matter © 2009 Elsevier Ltd. All rights reserved.
doi:10.1016/j.asd.2009.08.004

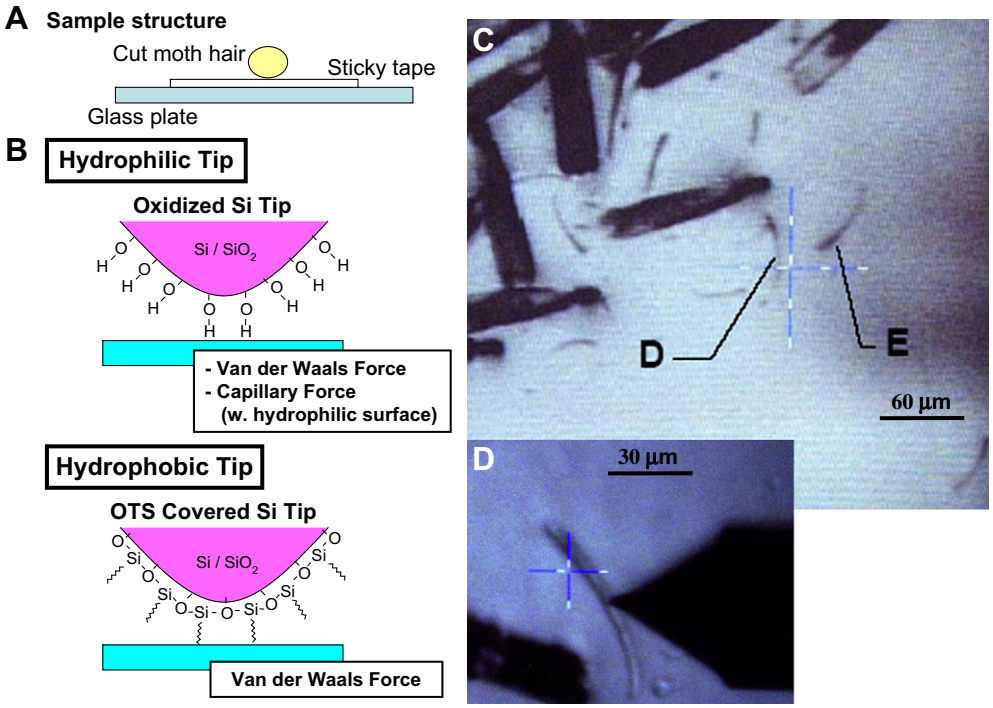

Fig. 1. A. Cross-section diagram of a trichoid sensillum sitting on the surface of sticky tape, ready for examination by the AFM tip. B. Two types of tips used for CFM scanning of trichoid sensilla. The SiO_2 tip (upper diagram) is a hydrophilic tip that when used under atmospheric conditions attains a monolayer of water distributed on its surface and is able to establish hydrogen bonds with surfaces that it probes during tapping mode. The tip that has been functionalized with OTS (lower diagram) is hydrophobic and is not able to establish hydrogen bonds with the surface that it probes in tapping mode. C. Light microscope image of the surface of the sticky tape with excised sensilla (marked D and E) plus scales that have sloughed off during piezo knife cutting of the sensilla. D. Light microscope image of the AFM tip ready to scan a sensillum.

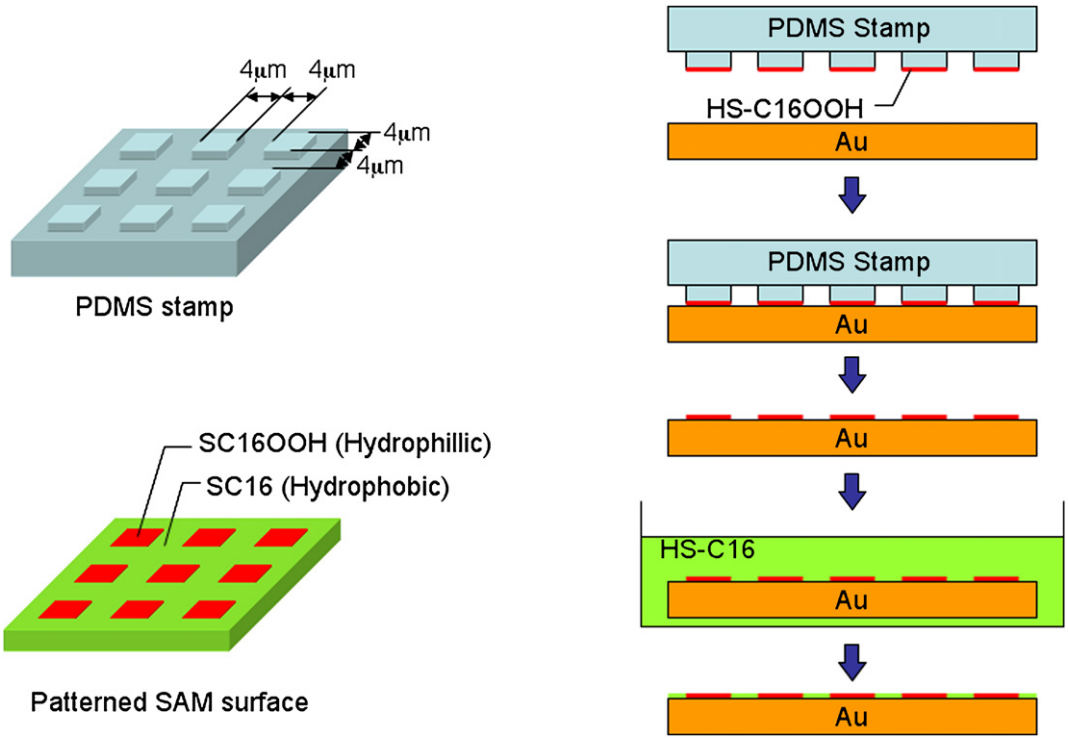

Fig. 2. Schematic diagram of the method for constructing a patterned surface on which to test the performance of the SiO_2 hydrophilic and OTS hydrophobic tips of CFM to ensure their hydrophilic or hydrophobic integrity, respectively. At right are sequential diagrams of the process in which the C15-COOH is stamped onto the gold surface and then C16 hydrocarbon is flooded onto the surface to fill in the areas between the 4 × 4 µm acid squares, eliminating height differences between the acid and the hydrocarbon areas of the surface. At bottom left is the end result, the test surface consisting of C15-COOH squares with C16 hydrocarbon in between.

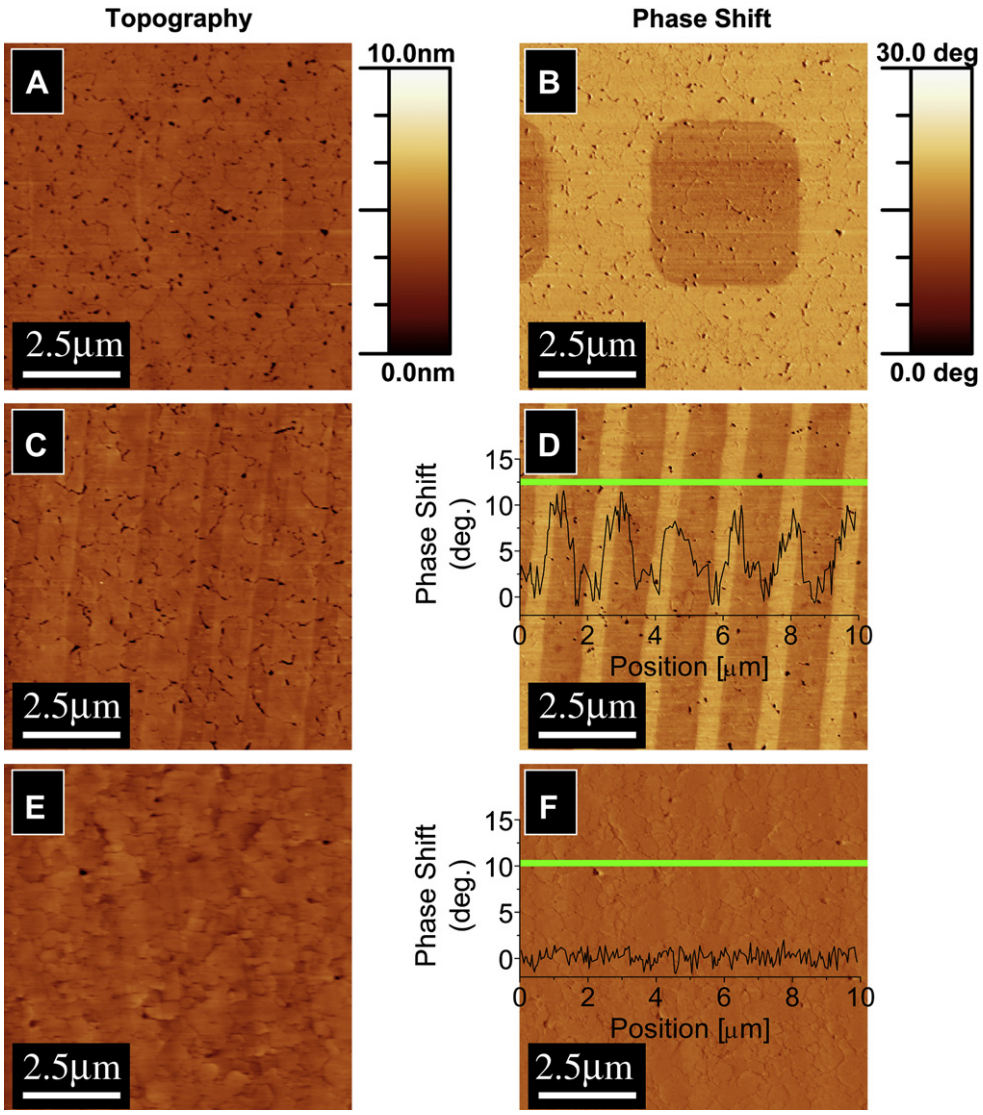

Fig. 3. A, C. CFM topographic images of surfaces stamped with squares (A) or stripes (C) of C15-COOH interspersed with C16 hydrocarbon using the SiO_2 hydrophilic tip, showing no height differences between the two types of chemicals on the surface. B, D. CFM phase-shift images of same surfaces taken simultaneously with A and C using the SiO_2 hydrophilic tip, showing strong phase-shifts (darker regions) when hydrogen bonding interactions occur between the SiO_2 hydrophilic tip and the acid terminated regions of the surface. Such images were used to confirm the integrity of each hydrophilic tip both before and after CFM scans of the trichoid sensilla were taken. E. CFM topographic image of surfaces stamped with stripes of C15-COOH interspersed with C16 hydrocarbon using the OTS hydrophobic tip. F. CFM phase-shift image of same surface taken simultaneously with E using the OTS hydrophobic tip, demonstrating that it exhibits no hydrogen bonding and confirming the success of the process creating this particular functionalized tip. Such images were used to confirm the integrity of each hydrophobic tip both before and after CFM scans of the trichoid sensilla were taken.

and facilitators that exist in the transporting of odorant molecules through the pore/pore-tubule system to reach the sensillum lumen (Steinbrecht and Müller, 1971; Steinbrecht and Kasang, 1972; Keil, 1982, 1984, 1987; Keil and Steinbrecht, 1987, 1992a,b).

In the sensillum lumen the pheromone component molecule is taken up by binding protein molecules and transported to odorant receptors (ORs) on the dendrite of the ORN in order to open ion channels in the dendritic membrane and trigger neuronal action potentials. The inner surfaces of the pores and the pore tubules are believed to consist of the same lipid layer that in transmission electron micrographs is electron-lucid and also covers the more electron-dense cuticulin layer of the epicuticle of each hair (Steinbrecht, 1997, 1999). The lipids of the epicuticle and pores are thought to protect the cells from water loss, but can also serve to facilitate the adsorption of odorant molecules (Locke, 1965).

The chemical composition of the cuticular lipids on insect sensilla had been tacitly assumed to be no different than the lipids coating any other cuticular surface of an insect. However, some evidence was raised that trichoid sensilla may preferentially adsorb pheromone molecules due to their different surface physical–chemical properties (Kanaujia and Kaissling, 1985). Calculations indicated that of the tritium-labelled sex pheromone odorant molecules that were puffed onto the male antennal surfaces, 80% quickly ended up on the long trichoid hairs (Kanaujia and Kaissling, 1985); these are the only sensilla that house pheromone-responsive ORNs. This differential adsorption occurred despite the fact that trichoids themselves make up only 20% of the antennal surface area. Kaissling (2004) dubbed this hypothetical surface chemistry phenomenon to function as an "olfactory lens" that would focus pheromone molecules onto the sensilla containing their pheromone component-tuned ORNs rather than letting them adsorb to other non-responding antennal surfaces and be lost to detection. Other calculations indicated that it only takes ca. 5 ms for pheromone molecules to arrive in the inner sensillum lumen from the

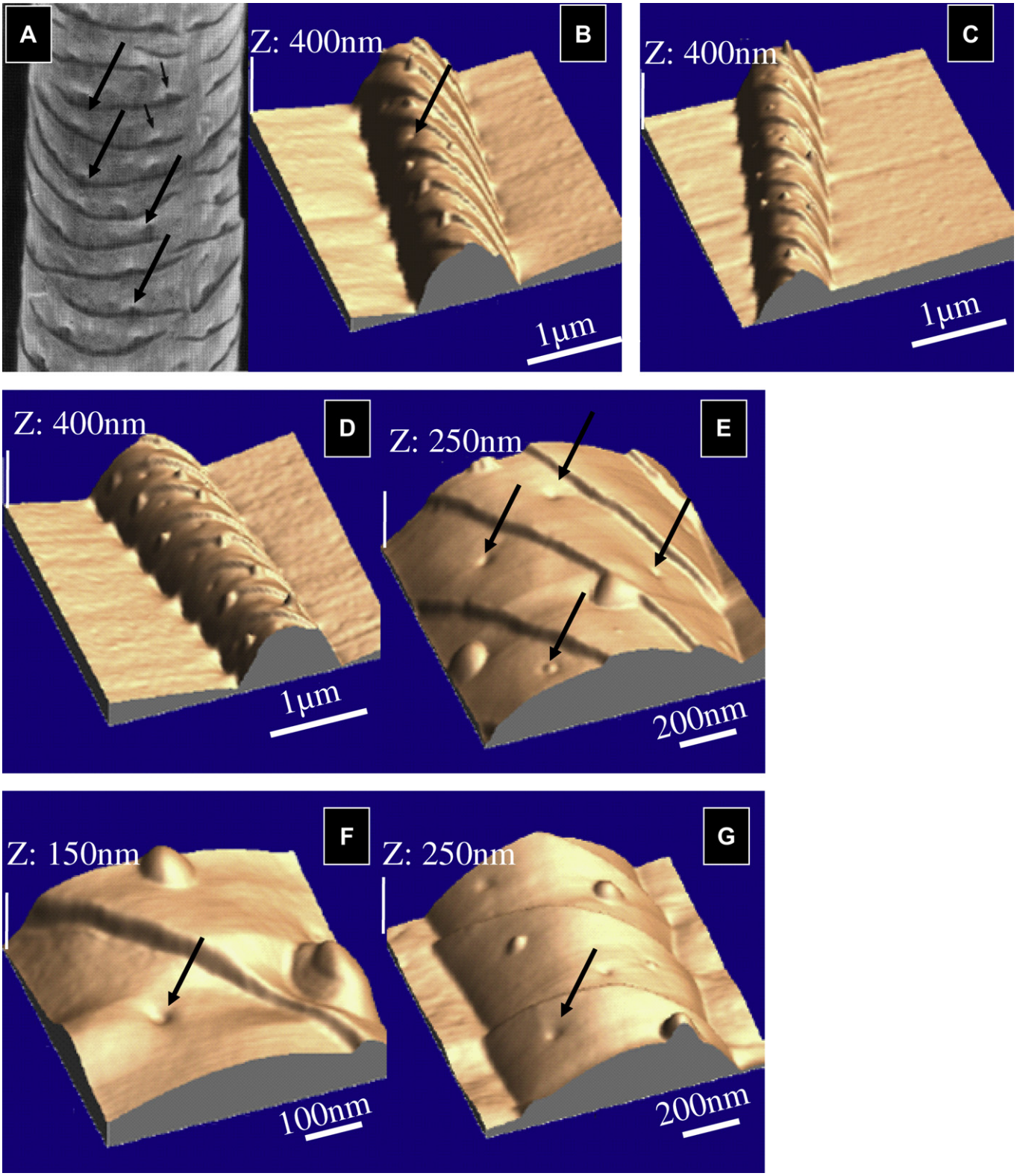

Fig. 4. A. Scanning electron micrograph image from Steinbrecht (1999) of a trichoid sensillum of *Bombyx mori*, showing numerous pores (arrows) and ridge structures. B–D. Topographic images from AFM scans of three different *H. zea* trichoid sensilla showing regular ridge structures and pores (arrow). E–G. Higher magnification topographic images of three other *H. zea* sensilla, showing pores (arrows) that appear either as depressions or with a dome of material over the depression. Note that some 3D images (B–D) contain an artificial aspect of distortion in the *Z*-axis, because the *Z*-axis' and X–Y axes' scales are different and cannot be reconciled with current software. This is a common occurrence for current AFM 3D displays.

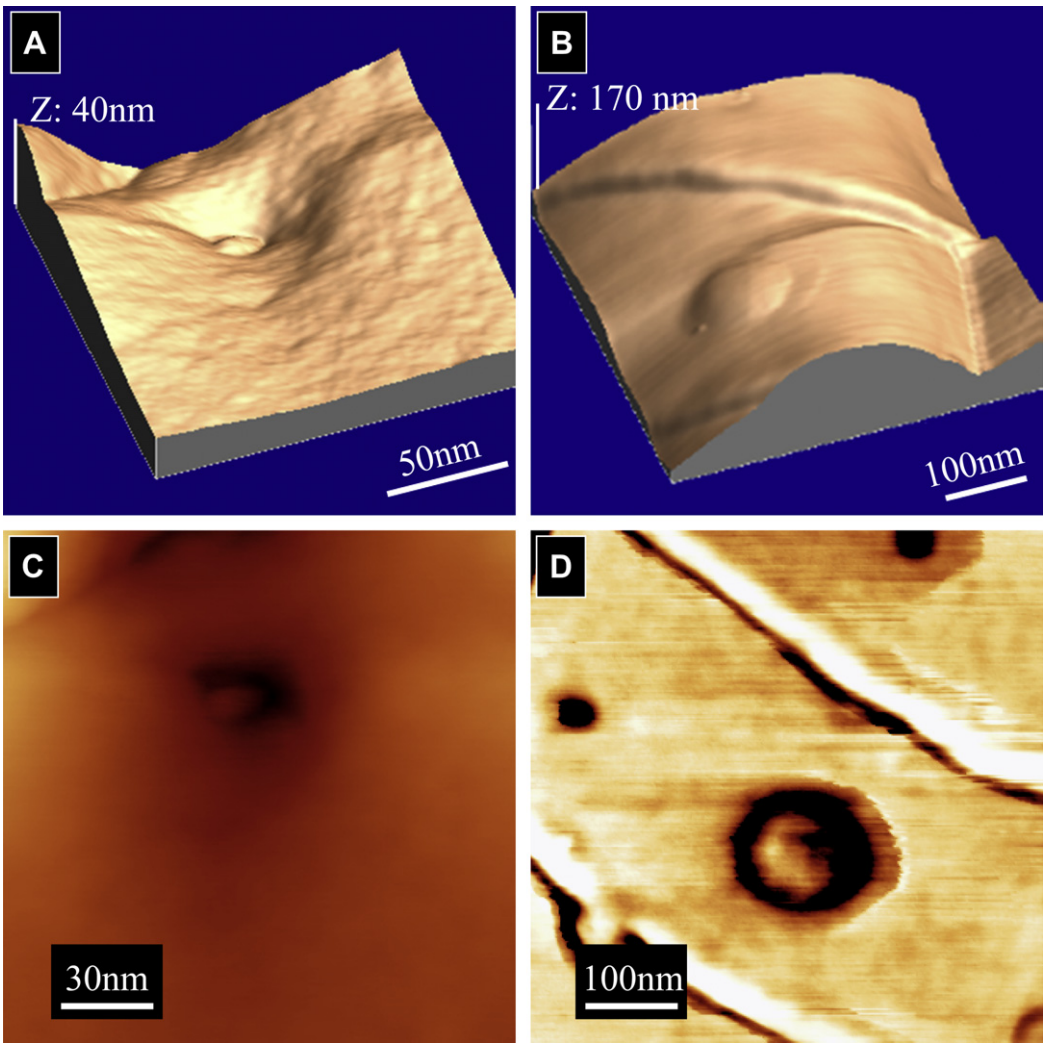

Fig. 5. A, B. CFM topographic high magnification images of a pore, (A) and a pore and a ridge (B) on two different *H. zea* trichoid sensilla. In A a small dome sits in the pore depression and in B a large dome entirely covers the pore. C, D. CFM phase-shift images of the same two areas of the sensilla simultaneously taken with A and B using the SiO_2 hydrophilic tip showing strong phase-shifts (darker areas) on or around the pores. The domes, as well as the top edge of the ridge in D, exhibit weaker or no phase-shifts indicating their surface chemistry is less conducive to creating hydrogen bonding with the tip.

time of their first contact with the lipid surface of the exocuticle (Kaissling, 2004; Kanaujia and Kaissling, 1985). This would require an extremely favorable physical chemistry environment for pheromone–surface lipid interactions.

We became interested in renewing investigations of pheromone capture by the surfaces of male trichoid sensillar epicuticular lipids and their possibly selectively adsorptive properties for different classes of pheromone molecules. In order to begin exploring the olfactory lens idea of Kaissling (2004), we first initiated studies to determine whether the lipid composition of the antennae of male moths might be different from that of other male cuticular body parts and also from the composition of female antennae. We found that in *Helicoverpa zea* moths, there were in fact slight but significant differences in the lipids on male antennae compared to those of females (Böröczky et al., 2008). These could be attributed to the trichoid sensilla that exist in huge numbers on male antennae but not on female antennae. Thus at the macro-level we found evidence for differential coating of the sensilla trichodea cuticular surfaces, not only between males and females but also between the male antennae and other body parts that might be attributed to selection for adsorption of pheromone molecules onto the male antennal surfaces (Böröczky et al., 2008).

In the present study we have now sought to determine whether there might exist heterogeneity of the lipid coatings on single trichoid sensilla that might give clues as to how pheromone molecules' adsorption onto, and transport through, sensillar cuticular walls might be expedited by a lipid-based nano-focusing of the pheromone molecules into the pores from non-porous areas of the sensilla. We used atomic force microscopy (AFM) to determine the nano-terrains of individual trichoid sensilla, and then used chemical force microscopy (CFM) to probe for differences in chemical bonding forces that could indicate differences in lipid coatings on different regions of the sensillar surfaces. Finally, we compared the results of these examinations of *H. zea* trichoid sensilla with those from trichoid sensillar from an unrelated species, *Utethesia ornatrix* that uses hydrocarbon sex pheromone components instead of aldehydes.

2. Materials and methods

2.1. Insects

The *H. zea* colony was maintained on a 16:8 L:D photoperiod at 25 °C, 40–50% RH. Larvae were reared on a modified pinto-bean diet (Shorey and Hale, 1965). Males and females were separated in

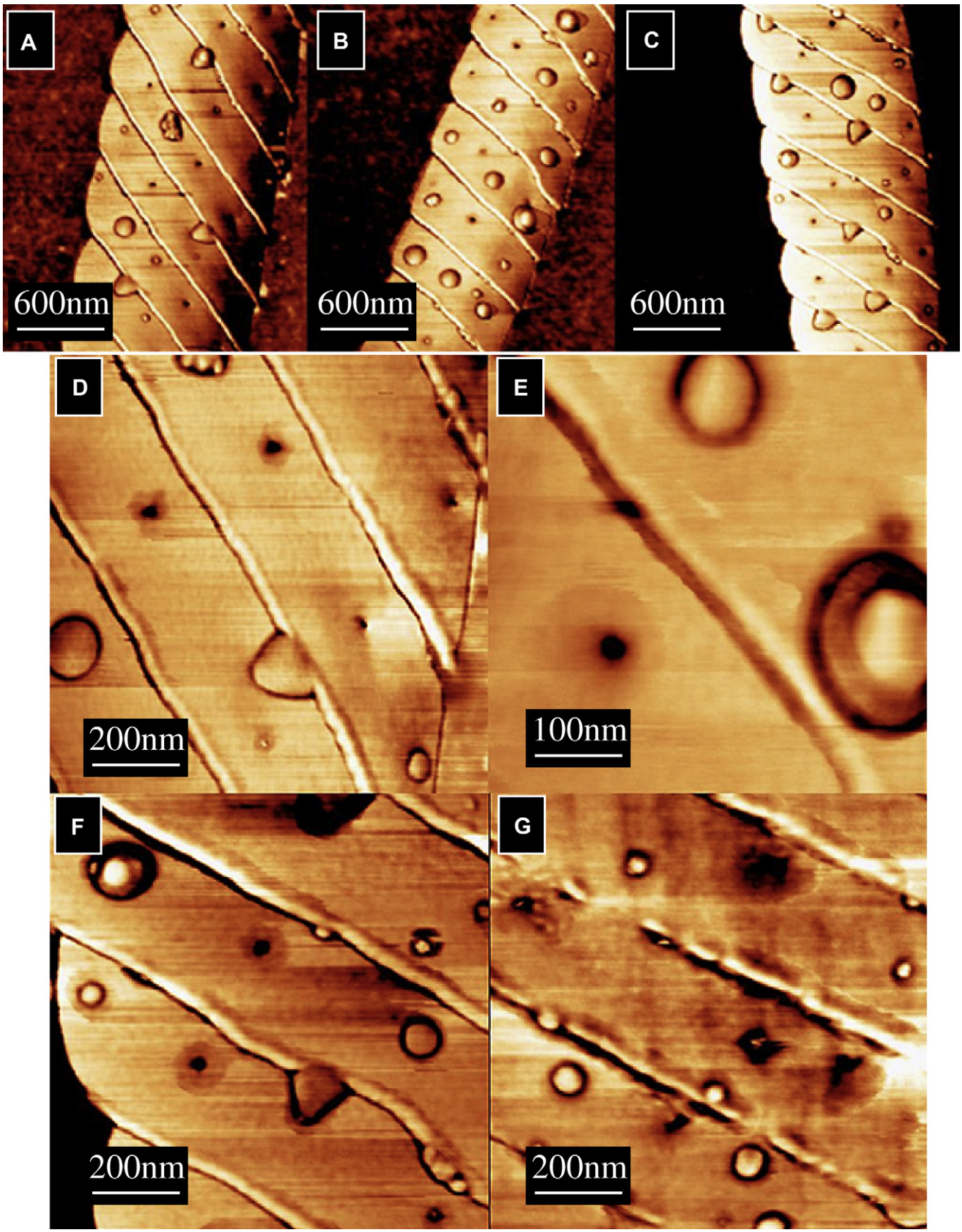

the pupal stage and housed in separate growth chambers in different rooms. The moths used in this experiment were males from 1 to 3 days old.

2.2. Preparation of isolated trichoid sensilla for AFM/CFM scanning

Trichoid sensilla were cut from male antennae using a vibrating, piezo-driven glass knife, following the technique of Hillier and Vickers (2007). Care was taken to try to cut the sensilla as close to their base as possible. The cut sensilla fell onto a double-sided sticky tape affixed to a glass microscope slide (Fig. 1A). Along with the sensilla, many scales from the dorsal side of the antenna came loose and stuck to the tape, but the sensilla could be located after some searching (Fig. 1C).

2.3. Brief description of AFM and CFM imaging techniques

Both of AFM and CFM imaging performed in this paper is based on the tapping mode AFM technique. In AFM imaging, a commercially available Si tip is used to scan the terrain of the surface in a raster pattern. The tip intermittently touches, "taps", the surface at the oscillation frequency of the cantilever to which the tip is attached. The cantilever including tip is controlled at a certain height from the surface, usually a few tens of μm (tip length: 15 μm, amplitude: 90–120 nm (RMS)), by a piezo x–y–z motor to achieve the setpoint amplitude of oscillation. When this value drifts from its setpoint, as when the tip encounters a ridge or valley, a piezo voltage change is applied to achieve the constant amplitude during the scanning, and thus the piezo voltage correcting the height of the tip above the surface is interpreted to be height data. A set of height data recorded throughout the scan provides a readout of the topography of the surface.

In CFM imaging, the same type of Si tip was used as in tapping mode AFM, but the tip's surface was chemically functionalized either by clean SiO_2 or hydrocarbon-based self-assembled monolayers (SAMs) to produce hydrophilic and hydrophobic tip surfaces, respectively. CFM is based on the same tapping mode AFM imaging technique but utilizes phase-shift analyses using chemically functionalized CFM tips. Therefore, the tapping frequency is driven by a driving piezo at the oscillation frequency, typically ~300 kHz, and the frequency of the cantilever is monitored by the deflection of the cantilever at a positional sensing detector located above the tip. The degree to which the tip's oscillations lag behind this driving frequency, i.e., a phase-shift, is also monitored during a tip scan. The amount of phase-shift is indicative of greater chemical interaction of the tip with the surface than if the interaction were neutral. Tip–surface interactions using hydrocarbon-coated, hydrophobic (lipophilic) SAM tips are generally attributed to only Van der Waals (VW) interactions with any surface. The tip–surface interactions with the SiO_2 hydrophilic tip, however, contain more intense hydrophilic–hydrophilic interactions that can be attributed to a capillary force, hydrogen bonding, or dipole–dipole interactions in addition to intrinsic VW interaction in cases in which the sensed surface is also hydrophilic. Therefore, the hydrophobic tip does not create phase-shift differences during interactions with either hydrophilic or hydrophobic surfaces. The degree to which the hydrophilic tip provides clear differences in phase-shifts depends upon the degree of hydrophilicity of the sensed surfaces.

2.4. CFM tip preparation

CFM images were obtained using the tapping mode of AFM with two types of tips; a hydrophilic tip and a more hydrophobic tip as shown in Fig. 1B. A Si (silicon) tip for tapping mode was used (Advanced TEC™ [Advanced Tip at the End of the Cantilever; silicon SPM Sensor], NANOSESSORS™, NanoWorld AG) and was prepared as a hydrophilic tip having a tip radius of ca.10 nm. During tapping the resonance frequency was ca. 300 kHz. The surface of the Si tip is normally covered by native silicon oxide (typically a few nm) from the atmosphere. To remove intrinsic organic contamination from the environment and prepare thicker oxide, the Si tips were immersed in piranha solution (3:7 of hydrogen peroxide and sulfuric acid) for 3 min, rinsed with water and ethanol, and exposed under UV/ozone cleaner (UVOCS, UVOCS Inc.) for 1 h followed by rinsing with ethanol and drying under N_2. After preparation of the SiO_2 hydrophilic tip, AFM images were taken within 4 h to avoid contamination that degrades hydrophilicity of CFM tips.

The same Si tip, Advanced TEC™, was functionalized as a hydrophobic tip by coating the tip surface with a 1-octadeciltrichlorosilane (OTS) SAM using the following procedure as shown in Fig. 1B (Allara et al., 1995; Parikh et al., 1994). The OTS SAM coating was prepared on both Si tips and Si wafers simultaneously to characterize the SAM and confirm its quality, since there are many reports that state that OTS SAM cannot be assembled straightforwardly compared to the commonly used SAM employing thiolate compounds on Au (Allara et al., 1995; Parikh et al., 1994; Ulman, 1996). For the solvent purification step, carbon tetrachloride (anhydrous, 99.9%, Aldrich) was distilled under N_2 and hexadecane (anhydrous, 99.9%, Aldrich) was run more than five times through a silica gel column activated by concentrated sulfuric acid to remove water prior to preparation of the OTS solution. The solution was prepared in a humidity controlled chamber equipped with both humidifier and dry N_2 flow to keep the relative humidity at 20–30% under room temperature. The OTS solution to prepare the SAM was composed of 20 μL of 1-octadeciltrichlorosilane (anhydrous, 95%, Aldrich), 4 ml of carbon tetrachloride, and 16 ml of hexadecane in a Teflon jar. The OTS solution was stored for aging under dry N_2 for 24–48 h prior to SAM preparation.

To prepare the OTS SAM, consecutive cleaning procedures were applied to both Si wafer substrates and commercially available Si AFM tips. The Si wafer functioned as a reference substrate to characterize the OTS SAM in terms of thickness by ellipsometry, infrared spectra by transmission mode infrared spectroscopy (IRS), contact angle measurement by water and hexadecane droplet, and surface topography by tapping mode AFM. Si AFM tips and Si substrates were exposed under the UV/ozone cleaner for 30 min, rinsed with ethanol, and dried under N_2 flow. Subsequently these were immersed in piranha solution for 3 min, rinsed with water five times, and then dried under N_2 flow. For Si wafers, ellipsometry, IRS, and AFM measurements were performed after 2 min immersion in the piranha solution in order to characterize the bare Si substrate. After characterization, the Si wafer was immersed in the piranha solution again for 1 min, rinsed with water, and dried under N_2 flow. Immediately after cleaning, Si substrates were immersed in the OTS solution for 50 min under atmospheric N_2. After SAM assembly, the OTS-coated Si substrates were immersed 3 times in distilled carbon tetrachloride for 10 min under N_2 in order to rinse extraneous OTS solution from the Si substrates. Results of

Fig. 6. CFM phase-shift images of three different trichoid sensilla using the SiO_2 hydrophilic tip, illustrating the various conditions of the pores (domed or un-domed) as well as the consistently lower phase-shifts (light lines) of the tops of the ridge edges, indicative of greater hydrophobicity of the ridge edges than the flat, planar inter-ridge areas. A–C. Views of the three sensilla showing the design of repetitive ridges and regular distribution of pores in the planar inter-ridge regions. Pores exhibit either large, small, or no domes. D–G. Higher magnification images of the same sensilla as in A–C. The pores, with or without domes, rarely occur along ridge-bases, and again the crests of the ridges exhibit lower levels of hydrogen bonding with the SiO_2 hydrophilic tip.

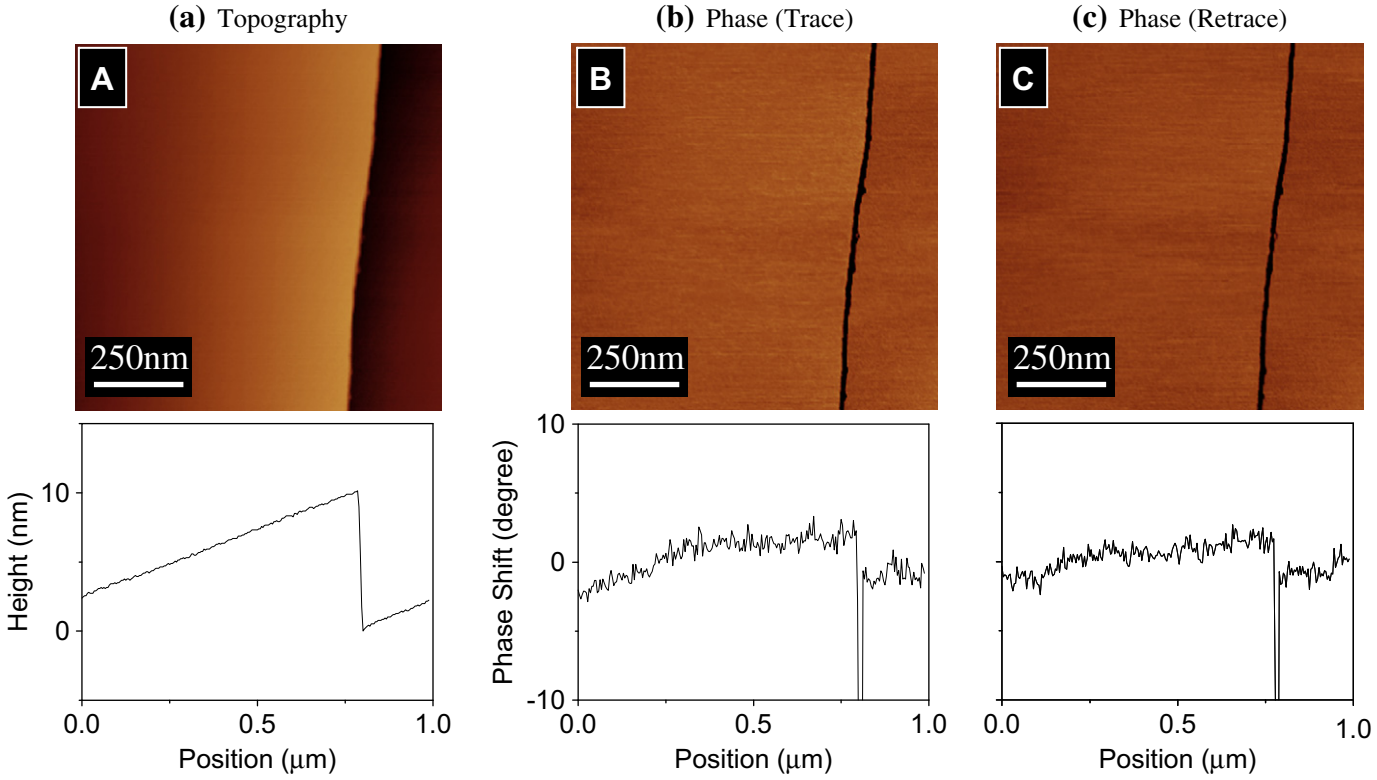

Fig. 7. A (upper). CFM topographic image of a freshly cleaved mica surface using the SiO_2 hydrophilic tip, illustrating a rise in height (increase in lightness) as the edge of the ridge is approached and a sharp decrease in height (dark regions) as the tip drops off the edge into the valley below during its scan. A (lower). Height data showing the rise and fall of the tip in cross-section during a scan. B, C (upper). CFM phase-shift images using SiO_2 hydrophilic tip taken during left-right scans (B) and right-left scan retraces (C) of the same cleaved mica surface as in A. No significant phase-shifts were observed with the rise and fall in height of the flat planar regions (no change in lightness or darkness). However a large phase-shift (dark line) occurred along the base of the ridge in both scans, indicating greater interactions of the tip as the sharp step increase of the ridge-wall was encountered, probably due to the sides of the tip rubbing against the wall. B, C Lower: The intensity of phase-shift (degrees) during left-right and right-left scans, respectively.

characterizations of SAM on Si surface revealed that the OTS SAM quality was sufficient to cover the Si tip surface. The degree of hydrophobicity of these functionalized AFM tips used in our CFM imaging was repeatedly assessed during the imaging of the moth sensilla as described in the following section. Because this CFM imaging mode is a tapping mode, we presume that the actual radius of curvature of the OTS-functionalized CFM tip was ca. 20 nm and convoluted with the real topographic features in case the range of features is around the tip size.

2.5. Verification of functionalized tip

The prepared hydrophilic and hydrophobic tips were verified by taking tapping mode CFM images of a hydrophilic and hydrophobic patterned surface made of carboxylic acid and methyl terminated long chain alkyl thiolate SAMs on Au substrate (Fig. 2). The patterned SAMs were prepared by a micro-contact printing (μ-cp) method using a stamp made of poly-dimethyl siloxane (PDMS) (SYLGARD 184 silicone elastomer, Dow Corning)(Michel et al., 2001; Whitesides et al., 2001). The μ-cp process with the PDMS is based on ink printing. The solution of 16-mercaptohexadecanoic acid (90%, Aldrich) (C15-COOH) was ink-printed to create a SAM on the Au surface; the rest of the bare Au surface was backfilled with 1-hexadecanethiol (99% Aldrich) (C16).

We used patterned photo resist (ca.1 μm thick) for a master of PDMS to be cured at 150 °C for 12 h under atmospheric N_2.A scheme of μ-cp process to prepare the patterned SAMs is shown in Fig. 2. The surface of the stamp was exposed under UV-Ozone cleaner for 2 min and rinsed with ethanol to make the PDMS surface have a high affinity for the carboxylic acid functional group of C15-COOH molecules in order to print the thiol functional group facing toward the printed Au substrate. After UV-Ozone exposure, the PDMS was immediately inked with a 1 mM solution of C15-COOH in ethanol, and then the PDMS was briefly dried under a N_2 stream for 30 s to remove excess amount of solution on PDMS. The inked PDMS stamp was pressed gently and uniformly onto freshly cleaved template stripped Au on a Si substrate for 30 s. The template stripped Au substrate is for obtaining robust flat Au substrate as reported elsewhere (Lee et al., 2008; Weiss et al., 2007). The stamped Au surface was immersed in 1 mM solution of C16 in ethanol for 5 min to backfill the bare Au surface. After being removed from the thiol solution, the sample was rinsed with ethanol and dried under a N_2 stream. The sample surface was then immersed in a 0.02 M solution of hydrochloric acid (36.5–38.0%, J.T. Baker) in ethanol for 1 min to remove the particle contamination due to dimerization of 16-mercaptohexadecanoic acid (Zhu et al., 2006), followed by rinsing with ethanol and drying under a N_2 stream. Representative CFM images of this hydrophilic–hydrophobic patterned SAM surface taken by both the hydrophilic and hydrophobic tips in tapping mode are shown in Fig. 3. That the OTS-functionalized tips had a coverage of more than 90% was confirmed for the hydrophobic AFM tips. All of tips used in CFM imaging of moth antennal sensilla surfaces were verified before and after their scans of the sensillar surfaces in order to confirm that the surface functionality of tips had retained their hydrophilic or hydrophobic integrities.

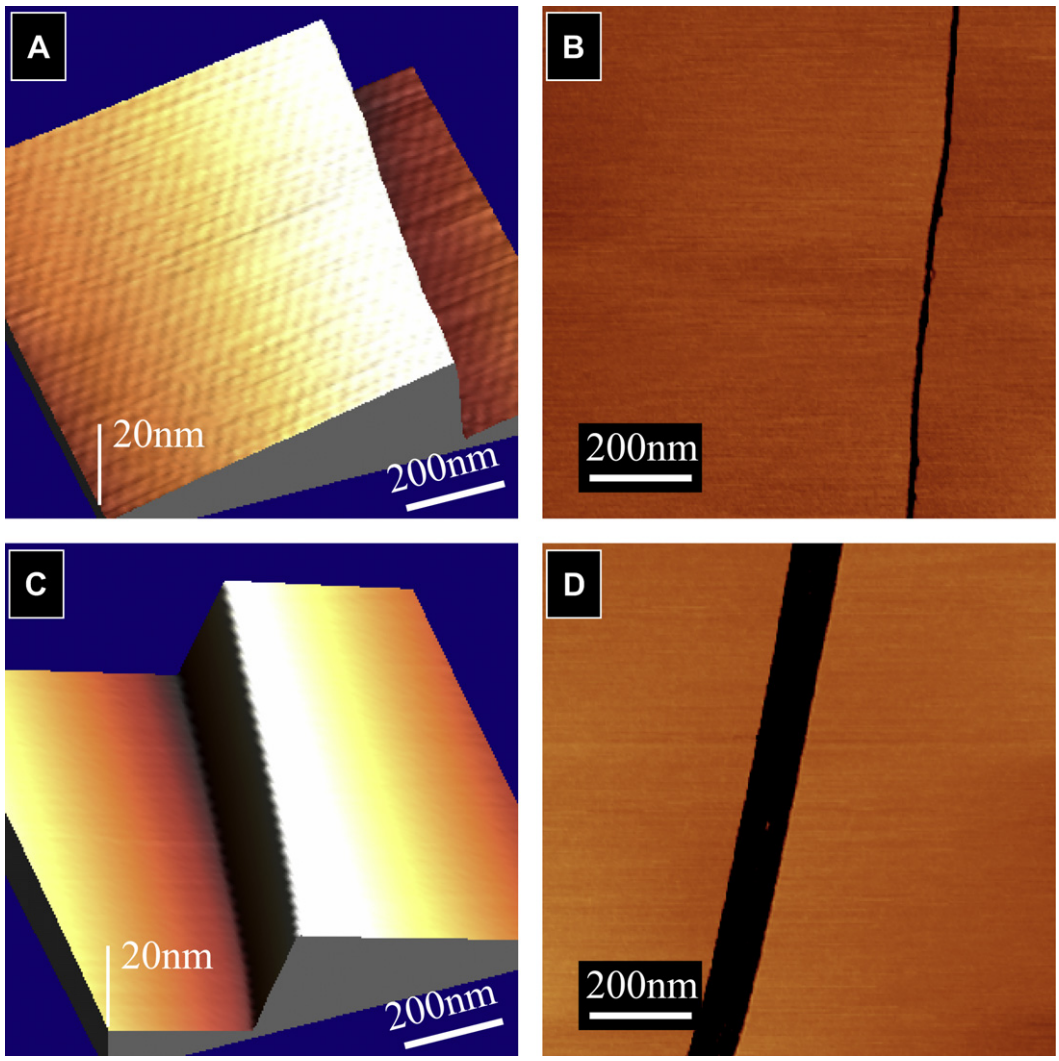

Fig. 8. A, C. CFM topographic images of two more cleaved mica surfaces using the SiO_2 hydrophilic tip, showing the extreme features of the much higher (lighter) ridges and the sharp drop-off to the valley below (dark areas). B, D. CFM phase-shift images using the SiO_2 hydrophilic tip, showing no phase-shifts (color changes) along the flat planar areas despite the severe rise and fall in height. There was no reduction in phase-shift (lightening of color) along the crests of the ridges, in contrast to the consistent lightening observed along the ridge-crests of *H. zea* trichoid sensilla. The reduced phase-shifting along the trichoid sensillar ridge-crests therefore is due to a difference in lipid composition or orientation along the crests compared to the planar regions. The intense phase-shifting (dark lines) along the bases of the ridges in B and D is likely due to the sides of the CFM tip rubbing against the walls of the ridge, creating a greater surface area for tip–surface interaction that creates an out-of-phase resonance. In D the width of the intense phase-shift (dark line) may be greater than in Fig. 7B and D or in Fig. 8B due to the more oblique angle the ridge-wall of this mica ridge rises from the base, causing a longer region of more intense tip–surface interaction during each scan.

2.6. Moth trichoid sensilla imaging using AFM and CFM

The topographic images and phase-shift images of trichoid sensilla for AFM and CFM images were created in the tapping mode AFM with a controller (Dimension 3100 SPM, Veeco Instruments Inc.) vibrating the cantilever arm at a resonance frequency of 250–330 kHz depending on the tips. The typical oscillation amplitude setpoint for the tip was within the range of 90–120 nm. The scanning speed across the surface for every size of image was 1 line/s.

During CFM imaging, the verification of tip quality in terms of either hydrophilicity or hydrophobicity was performed using the patterned SAM surface with C16 thiol and C15-COOH thiol both before and after imaging of the trichoid sensillum (Fig. 3). CFM images of trichoid sensilla taken with tips that did not show consistent before and after CFM image patterns were discarded due to the possibility that the tips' characteristics had become compromised during contact with the lipid coatings of the sensilla.

All phase-shift images of CFM shown in this paper have the same phase-shift range of $\pm 15^{\circ}$. Because phase-shift images produce complicated artifacts on unknown natural surfaces, the phase-shift characteristic as a function of the amplitude setpoint was always confirmed before starting the image acquisition of each trichoid sensillum in order to avoid a possible inversion of phase-shift image due to tip–surface interactions (Bar et al., 1997; Brandsch et al., 1997; Chen et al., 1998; Garcia and Perez, 2002; Haugstad and Jones, 1999). Images were confirmed to be consistent by taking images from at least 10 different moth sensilla. Because complex natural terrain such as sharp ridges might complicate the interpretation of some of the strong phase-shift attraction force interactions between the tip and surface due to the sides of the tip rubbing against such features, a freshly cleaved mica surface was imaged using hydrophilic tips to sample an extremely hydrophilic surface having sudden, steep step-edges similar in height (10–30 nm) to the step-edges of the trichoid sensilla (Figs. 7 and 8) in order to examine possible phase-shift artifacts due to extremely strong tip–surface interaction.

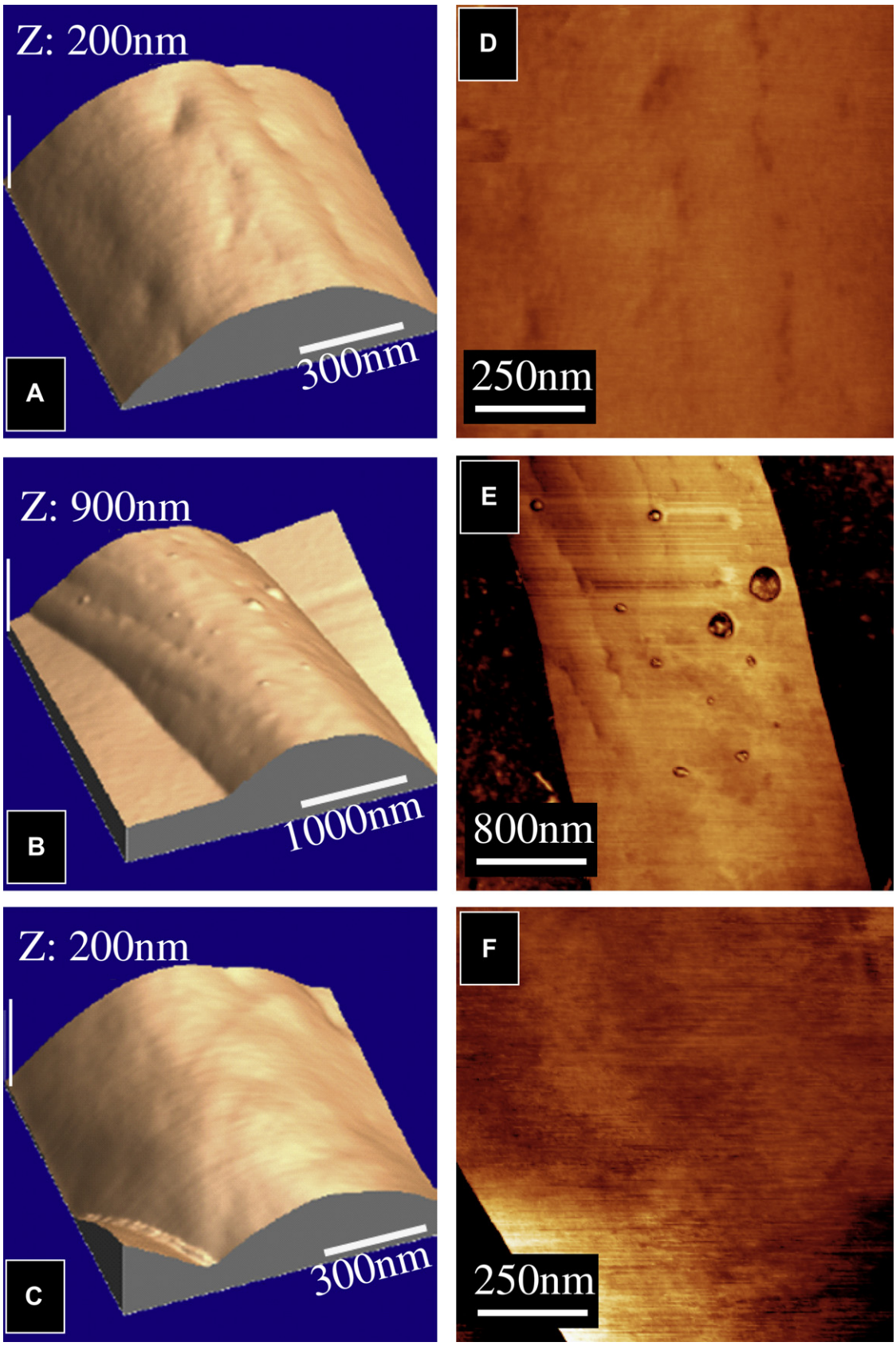

Fig. 9. A–C. CFM topographic images of the basal regions of three sensilla, showing the lack of pores and ridges basally. Note that some of the 3D images in A–C contain an artificial aspect of distortion in the *Z*-axis, because the *Z*-axis' and X–Y axes' scales are different and cannot be reconciled with current software. This is a common occurrence for current AFM 3D displays. D–F. Simultaneous CFM phase-shift images taken of sensilla in A–C using the SiO_2 hydrophilic tip, with the uniformity of coloration illustrating the lack of surface lipid heterogeneity in these basal sensillar regions.

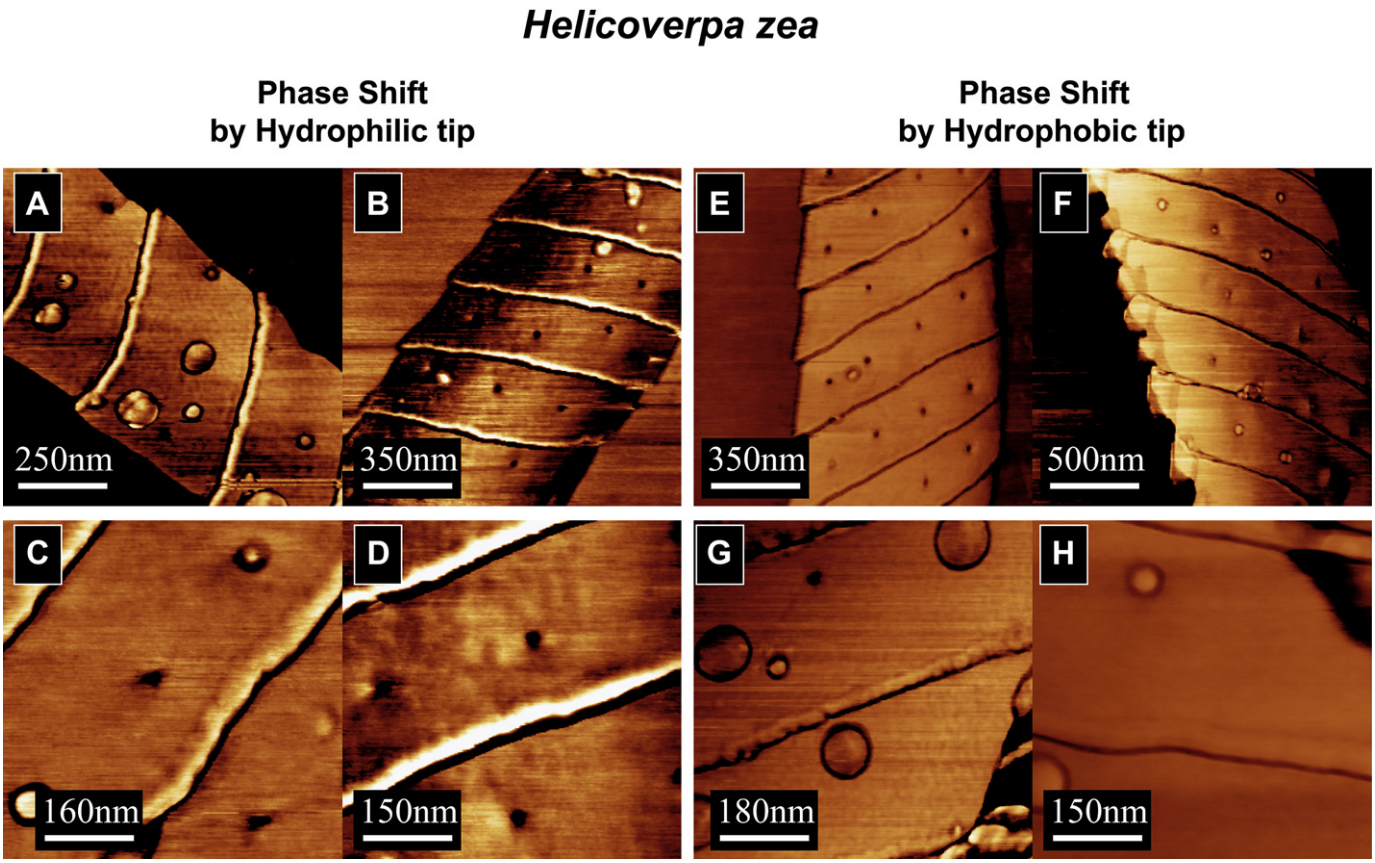

Fig. 10. A–D; CFM phase-shift images of four *H. zea* trichoid sensilla using the SiO_2 hydrophilic tip. Note the light areas along the ridge-crests indicating less hydrogen bonding, indicative of a different surface lipid composition or molecular orientation. E–H; CFM phase-shift images of *H. zea* trichoid sensilla using the OTS-functionalized hydrophobic tip; there are no light areas along the ridge-crests and the tip–surface interactions are uniform (in color) because no hydrogen bonding can occur. As in all other images, the dark bands (greater phase-shifts) running along the bases of the ridges are likely due to the sides of the tip rubbing against the walls of the ridges, resulting in greater interaction (friction) of a greater surface area of the tip with the sensillum surface, causing a phase-shift lower than the generated oscillation frequency.

3. Results

3.1. AFM imaging of the H. zea sensilla and CFM of a pore

AFM images of the trichoid sensilla of male *H. zea* antennae reveal multitudes of regularly space ridges around the sensilla that are interspersed with flat, planar regions of cuticle (Fig. 4B–G). The inter-ridge distance is usually ca. 300–500 nm. The planar inter-ridge surfaces appear to rise slightly to the edge of each ridge, then drop drastically by 10–30 nm to the base of the ridge, with the planar inter-ridge region rising again toward the edge of the next ridge, and so on. The effect is a saw-tooth pattern, like a step-series of rice paddies going up a hillside.

The smooth, flat, inter-ridge regions are populated with small, dimple-like depressions running midway between, and parallel to, the step-edges of the ridges (Fig. 4). These depressions are regularly spaced at 300–500 nm depending on which region of the sensillum they occur, and appear to be consistent with the olfactory pores on the trichoid sensilla of other species that have been confirmed as such through transmission electron microscopy (Fig. 4A) (Steinbrecht, 1997, 1999). These putative pore openings as imaged by AFM/CFM have a diameter of ca. 30 nm.

In a great number of cases, at a location where a dimple (pore) should be located, there is instead a dome of possibly lipid exudate that partially or completely covers the pore opening. These periodic domes vary greatly in diameter in unpredictable fashion from place to place on each sensillum. Some domes are of small diameter (ca. 10–20 nm) and remain inside the depression, giving a combined pit–dome configuration to the topography (Fig. 4E bottom; Fig. 5A). Others of larger diameter (>50 nm) completely cover the pore depression and generally rise to greater heights (Fig. 4E–G). The pit–dome pores are revealed in more detail in CFM phase-shift images (Figs. 5C,D,6 and 10 A–D) during tapping mode to have a possibly lesser degree of hydrogen bonding than the flat inter-ridge regions or the pore depressions on which they sit.

3.2. CFM imaging of H. zea sensilla and mica surfaces

CFM phase-shift images taken using the SiO_2 hydrophilic tip revealed in nearly every case that the cuticular surfaces on the crests of the step-ridges have less intense hydrogen bonding interactions with the tip than do the flat planar areas (Figs. 5D, 6, and 10A–D). Along the lengths of the bases of the step-ridges (the start of each inter-ridge flat region), large dark-shaded phase-shifts are always present, which indicates a stronger interaction of the surface with the CFM tip. Large phase-shifts also occur over each open pore and also at the perimeters of each dome-covered pore. Such signals constitute a combination of possible stronger chemical force interaction (greater hydrogen bonding) between the CFM tip and lipids on the sensillar surface, but potentially confounding interactions between the sides of the tip and the cuticle in these terrains make a purely tip-chemical-force interpretation difficult.

As a control, CFM scans of mica surfaces were taken using SiO_2 hydrophilic tip and compared. CFM topographic images of freshly cleaved mica show a clear lightening as the crest of the step–ridge is approached by the AFM tip (Figs. 7A and 8A, C). The lightening of

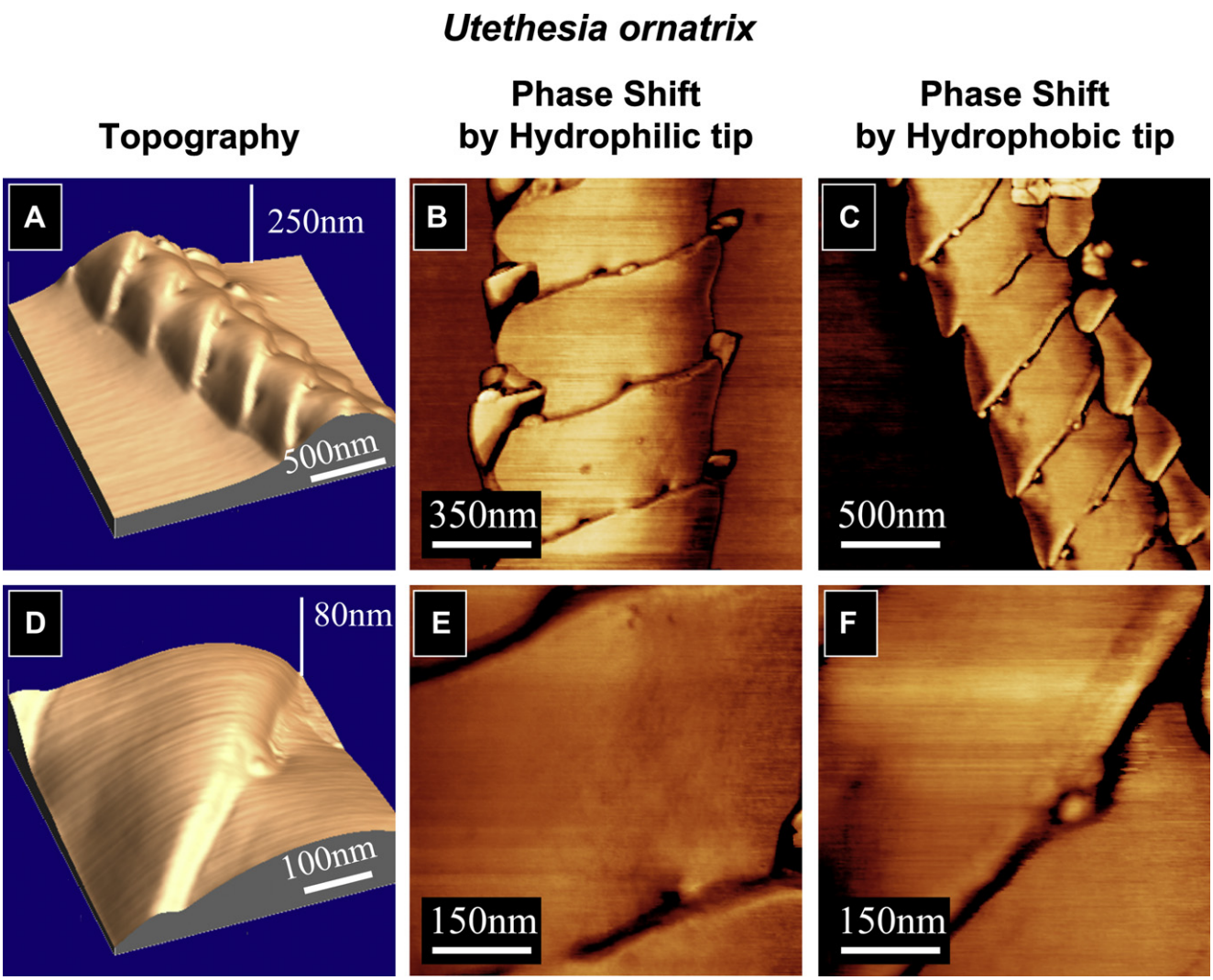

Fig. 11. A, D; CFM topographic images of two *U. ornatrix* trichoid sensilla using the SiO_2 hydrophilic tip at lower (upper panel) and higher (lower panel) magnifications, respectively. Note that pores, with and without domes, occur at the bases of the ridge areas, and not on the flat planar inter-ridge regions. B, E; CFM phase-shift images of two *U. ornatrix* trichoid sensilla using the SiO_2 hydrophilic tip. Note that there are no light areas along the ridge-crests indicating that for this species there is no indication that the surface lipid compositions or molecular orientations here make the surface any less polar than elsewhere on the sensilla. C, F; CFM phase-shift images of the same two regions taken simultaneously with A and D using the OTS-functionalized hydrophobic tip. Again, no light areas can be seen along the ridge-crests and this is as expected, since there was no indication using the SiO_2 hydrophilic tip that there is any polar lipid surface heterogeneity on this species' sensilla. As in all other images, the dark bands (greater phase-shifts) running along the bases of the ridges are likely due to the sides of the tip rubbing against the walls of the ridges, resulting in greater interaction (friction) of a greater surface area of the tip with the sensillum surface.

the image as expected corresponds to the increase in topographic height up to the crest of the ridge edge. In contrast, in CFM phase-shift images, there is as expected no lightening whatsoever at the ridge-crests (Fig. 7B and D) because there is no change in chemical composition of the mica along its surface. Thus in CFM phase-shift images of the step-ridges of *H. zea* sensilla (Figs. 5D,6,10A–D), the consistent lightening along each of the ridge-crests is indicative of weaker hydrogen bonding between the SiO_2 hydrophilic tip and the cuticular lipids along these crests than on the inter-ridge planar regions and is not due to a confounding of topography with chemical force as the tip travels over the crests. This is indicative of a different chemical composition or orientation of the cuticular lipid molecules along the ridge-crests.

The mica test surface CFM images show strong phase-shifts (dark lines) running along the valleys below the crests in the mica sheets (Figs. 7B,C and 8B,D). These results are indicative of strong tip–surface interactions occurring only in these valleys due to the sides of the tip interacting with the walls of the mica ridges and producing stronger interaction from this greater surface area of contact. These results suggest that the dark areas in CFM phase-shift images of *H. zea* trichoid sensilla at the bases of the ridges may likewise be due to greater surface area contact of sides of the tip when it encounters the sides of the steep walls of the ridges as it oscillates.

CFM topographic images also highlight the fact that on *H. zea* trichoid sensilla, the vast majority of pores, with domes or without, occur along the flat planar areas of the sensilla (Figs. 5,6 and 10). Occasionally, some features that appear to be pores or their domes occur along the bases of the ridges (Fig. 6). The strong (dark) phase-shifts occurring over what appear to be open (un-domed) pores on the flat inter-ridge regions may also be due to a greater surface area interaction caused by the sides of the tip contacting the sides of the pore opening when the oscillating tip dips down into the pore depression. Similarly, the dark circles around the domed pores indicating a greater phase-shift (Fig. 6) may be due to this same phenomenon of the sides of the tip simultaneously contacting both the side of the dome and the edge of the pore opening.

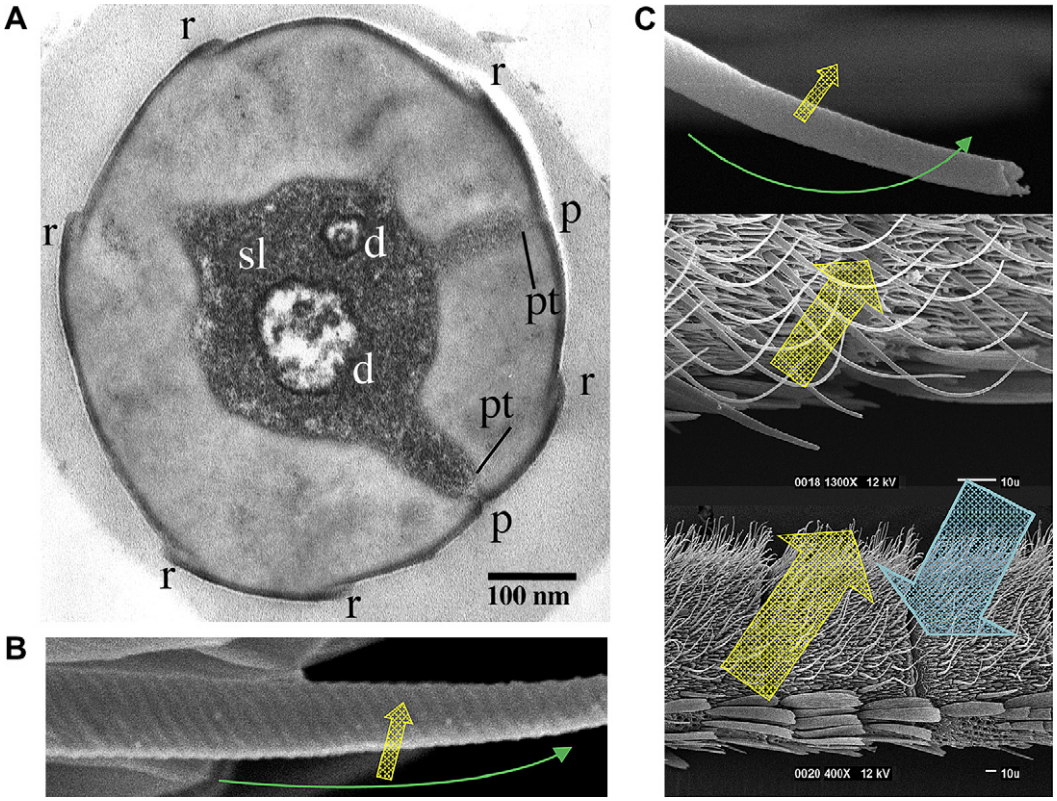

Fig. 12. A. Transmission electron micrograph of the cross-section of a *H. zea* trichoid sensillum. Note how the ridge-crests (r) overlap and ride above each flat planar region of the cuticle. One can see how inaccessible the sub-ridge areas are to AFM/CFM tips. Two pores (p) occur near the middle of two of the planar regions of cuticle. Two very faint, white pore tubules (pt) can be seen descending from each of the pore openings. There is a large and a small dendrite (d) in the lumen of this sensillum surrounded by sensillum lymph (sl). B. Scanning electron micrograph of a *H. zea* trichoid sensillum, showing how there seems to be a fixed relation between the hair axis and the stacked rings of ridges along the hair shaft related to the curvature of the tip. C. The distal ends of each trichoid sensillum will be curved forward in flight toward oncoming odor molecules, in the direction the moth is thrusting (light-colored arrows in direction of curvature of sensilla in B and C). Extra arrow in C (bottom panel) denotes direction of oncoming odor molecules. In the top panel of C, the normally pointed end of this sensillum had been cut, using a glass knife, in preparation for electrophysiological recordings.

It is noteworthy that the occurrence of pores was always coincident with the occurrence of ridges on these sensilla. Although pores were always observed along with ridges in the medial or more distal portions of the sensilla, no pores were observed in images of the proximal (basal) portions of the sensilla (Fig. 9A–C). Coincidentally, no ridges were observed basally. No obvious differences in hydrogen bonding interactions were seen in these basal regions in the scans of these smooth, ridgeless surfaces (Fig. 9D–F).

3.3. CFM imaging of H. zea and U. ornatrix sensilla

Like *H. zea* (Fig. 10), in CFM topographic images of *U. ornatrix* trichoid sensilla from male antennae exhibited step-ridges with regularly spaced pores (Fig. 11). One difference between the species is that the pores on *U. ornatrix* sensilla nearly always occur along the bases of the ridges (Fig. 11) rather than in the middle of the planar inter-ridge areas as they do in *H. zea*. The pores on *U. ornatrix* sensilla, as in *H. zea*, sometimes appear to have a dome that covers or partially covers the pore (Fig. 11C, D and F).

In CFM phase-shift images taken with SiO_2 hydrophilic tip, *U. ornatrix* trichoid sensilla exhibited no decreases in hydrogen bonding interactions along the crests of the ridges, as indicated by a lack of lightening of the images along the crests (Fig. 11B and E). In contrast, light areas are consistently observed along the step–ridge edges of *H. zea* antennae (Fig. 10A–D). Thus unlike *H. zea* sensilla, in *U. ornatrix* the crests of the ridge edges do not appear to have a different lipid composition or molecular orientation than the flat inter-ridge regions.

In contrast to these SiO_2 hydrophilic tip CFM scans, when the possibility of hydrogen bonding interactions was eliminated by using the OTS-functionalized hydrophobic tip, for both *H. zea* and *U. ornatrix* the OTS tip CFM phase-shift images exhibited no differences in tip-cuticle chemical forces along the crests of the ridges compared to the planar surfaces between ridges (Figs. 10E–H and 11B,C,E and F). These OTS hydrophobic tip results compared to those using the SiO_2 hydrophilic tip indicate again that for *H. zea* the step–ridge edges differ in chemical composition or molecular orientation from the planar surfaces. In contrast, on the *U. ornatrix* sensilla the lack of differential interaction with either the SiO_2 or the OTS along the crests of the ridge edges indicates that the lipid layer surfaces of its trichoid sensilla are more uniformly coated across all areas.

4. Discussion

The sensilla trichodea of *H. zea* males appear to exhibit a nanoscale-level of heterogeneity with regard to the types of lipids or the orientations of the lipid molecules that are distributed across their surfaces. CFM analysis revealed regular variation in the amount of hydrogen bonding that occurred between the surface lipids and the SiO_2 hydrophilic tip, with all of the crests of the step-ridges exhibiting weaker hydrogen bonding with the tip than the flat inter-ridge surfaces.

The physical chemistry of odor molecule adsorption at the antennal–sensillar level will depend on diffusion and not on fluid flow (Loudon and Koehl, 2000). Because diffusion predominates at the nano-level close to sensilla, we can conjecture that such heterogeneity in lipid chemistry could have significant effects. Although it is not known how pheromone component molecules might interact with sensillar lipid coatings during initial adsorption from the air onto the sensillar surface, it is possible that a heterogeneity of lipid coatings might help focus pheromone molecules to their target pores. The regular spatial disparity in polarity might even cause the molecules to be forced toward the more favorable pore regions than to the ridges before they come into contact with the surface.

The relatively lower amount of CFM phase-shift on the step–ridge edges was not due to their higher topography because scans of mica surfaces that had a similar height disparity as the *H. zea* ridges and troughs displayed no such phase-shift changes along their step-ridge edges (Figs. 7 and 8). Moreover, eliminating the possibility of hydrogen bonding by using a CFM tip that was coated with a monolayer of octadecyl-hydrocarbon caused the difference between the tip interactions at the step–ridge edges and the flat planar regions of *H. zea* sensilla to disappear (Fig. 10E–H).

Even the AFM topographic analyses suggest that the ridges on these and other moths' trichoid sensilla may play a significant role in pheromone component adsorption from the air onto the sensillum. Pores only occur in conjunction with ridges; the basal regions of sensilla contain no pores and they also have no ridges (Fig. 9). If the construction of a trichoid sensillum during development required that the cuticle be extruded out into a long hair-like geometry comprised of stacked, equidistant ringed ridges (Fig. 12B), then it is logical to assume that the ridges should be present along the entire length of the hair, including the base. However, the consistent juxtapositioning of ridges with pores would argue that ridges have had a selective advantage related to signal focusing that aids pheromone molecule adsorption into the pores. Otherwise, ridges should appear everywhere on the sensillar surface. The repeated stacked-ring occurrence of the ridges along the sensillum seems to be involved with the sensillar tip curving forward to intercept odor molecules during flight (Fig. 12B).

Nearly all of the *H. zea* sensillar pores that we were able to visualize in the images from our AFM and CFM scans are regularly spaced along the flat planar areas. A very high proportion appear as simple depressions having a diameter of ca. 30 nm. However, many other pores are partially or completely covered by various-sized lipid domes. We do not know if these domes also occur in vivo, or whether they are artifacts of cutting the sensilla for examination. A few such domes can be seen in scanning electron micrographs of silkmoth trichoid sensillar pores from intact sensilla residing on antennae (Steinbrecht, 1999).

If the domes do occur in vivo, it is anybody's guess as to their function in pheromone component adsorption and surface diffusion. Our CFM analyses indicate that they may be slightly more hydrophobic than the planar surfaces due to their oftentimes lighter appearance than the flat inter-ridge areas (Figs. 6 and 10). Locke (1965) considered the domes that generally occur over pore canals all over the insect body as the occurrence of two different orientations of polar lipid molecules that he envisioned as comprising the "organized lipid layer" of the epicuticle. He viewed these polar lipids as existing as a liquid crystal layer beneath the outermost, cement layer. For olfactory sensilla, transmission electron micrographs (Steinbrecht and Kasang, 1972; Keil, 1982, and reviews by Steinbrecht, 1987, 1997, 1999) supported the idea of three layers in the epicuticle of olfactory sensilla, and focused on the electron-lucid L2 layer as the one layer that is contiguous between the flat surfaces and channels of the pores and associated pore tubules. This layer was felt to be the key lipid layer involved in the adsorption of odorants and their entry into the lumen of the sensillum (Steinbrecht, 1987, 1997, 1999).

We suggest that our CFM images that show some pores having domes and others lacking them could possibly be due to two different orientations of polar lipids occurring at the pore entrances that had been envisaged by Locke (1965). One orientation would allow strong phase-shifting interactions with the tip and appear as an "open" (dark) pore, whereas the other would diminish these interactions and appear as a dome, often with a very light, lipophilic shading in CFM images (Figs. 6 and 10). The AFM/CFM topographic images show some pores having very slight or no domes, and therefore some of the pores may have much more lipid exudate at the pore opening than others.

We are unable to suggest anything concerning the chemical properties of the pores themselves based on our CFM probings of the *H. zea* sensillar surfaces, because although our CFM analyses using the SiO_2 hydrophilic tip seem to indicate that the non-domed pores may be more hydrophilic than the planar areas, the strong phase-shifts observed over each pore are confounded by a greater surface area of tip-cuticle interaction as the tip dips down into the pore and its sides contact the pore walls as observed with OTS hydrophobic tip (Fig. 10E and F). Thus, possible differences in molecular composition or orientation of the lipid molecules at the pore opening compared to those on the planar surfaces cannot be inferred. CFM scans of mica surfaces also reveal a predictable phase-shift darkening of the signal at the bases of the ridge edges. These images suggest that there is more of an interaction of the sides of the CFM tip with the walls of the mica step-ridges when the tip is near the base of the ridge, especially if the ridge-wall rises at an oblique angle from the base (Fig. 8). Once a way can be found to factor out these confounding factors and determine the relative hydrophobicity of the open pore lipids compared to the flat inter-ridge regions or the step–ridge edges, we can form better hypotheses about what's happening during these initial stages of pheromone odorant adsorption into the pores and the contributions of other lipid surfaces of the sensilla.

We cannot determine from either the AFM or CFM scans whether there are possibly more pores that occur at, or under, the bases of the ridges because neither of the probe tips can gain access to the cuticle at the ridge-base areas in order to sample under there. Our transmission electron micrographs of *H. zea* trichoid sensilla show that the flat planar regions are overlain by the crests of the ridges (Fig. 12A). In such TEM images of *H. zea* or in other moth species (Steinbrecht, 1997, 1999), pore structures underneath the crest-plane junctions have not been observed. However, we cannot eliminate the possibility that some adsorption and transport of pheromone molecules could possibly be occurring directly through the cuticle via poreless transport (Steinbrecht, 1987) into the sensillum lumen underneath the ridge-crests.

One can imagine that the mixture of lipids (Böröczky et al., 2008) that is secreted out through the pore tubules by the trichogen, thecogen, or tormogen support cells and that coats the cuticular surface during development (Keil and Steiner, 1991; Keil, 1997) must undergo a great degree of self-assembly. Lipids of different classes might partition themselves onto pore or ridge areas according to molecular type, and in addition they may assume different orientations depending on the topography of the substrate to which they are bound and according to chemical forces that may uniquely occur at nanoscale levels, such as within pores (Locke, 1965). We have shown here that there is nanoscale molecular heterogeneity, either of composition or molecular orientation, in the lipid molecular coatings covering single trichoid sensilla.

At the more macro-scale, we previously provided evidence that the lipid composition of *H. zea* trichoid sensilla differs from that of

other sensilla, based on comparisons between the lipid compositions of male versus female *H. zea* antennae (Böröczky et al., 2008). Such differential coating of trichoid sensilla could contribute to an "olfactory lens" effect (Kaissling, 2004) that focuses the adsorption of pheromone molecules preferentially onto their target sensilla rather than elsewhere on the antennal surface. Although the surfaces of pheromone component-related sensilla may have been under strong selection pressure to be preferentially endowed this way for optimal pheromone component capture, we do not think that the cuticular lipids on all types of olfactory sensilla would have similar degrees of specificities of lipid coating. On the contrary, evidence shows thus far that in *Drosophila melanogaster* neither the lipid coatings nor binding proteins of antennal basiconic sensilla housing general odorant receptors (ORs) play any significant role in altering either the odorant response profiles or the temporal firing patterns of ORs that are transgenically expressed on a non-native receptor neuron housed within a non-native basiconic sensillum (Hallem and Carlson, 2006). Their results make it difficult to imagine that for general odorant olfaction there is any specificity of odorant adsorption onto the sensillum surface that is imparted by perireceptor factors such as cuticular lipid coatings. However, it may still be possible that this general lipid mixture may differentially self-assemble across basiconic sensillar cuticle and its spatial heterogeneity serve to focus general odorant molecules into the sensillum lumen.

The pheromone component molecules of most species of moths that have been identified to date have a functional group such as an acetate, aldehyde, or alcohol at one end and a long lipid chain at the other, and could possibly function as a surfactant. Thus the pheromone may possibly solubilize within the L2 lipid layer and not just change from 2D to 1D surface diffusion from the sensillar surface down into the pores and pore tubules (Adam and Delbruck, 1968).

A smaller but still significant number of moth species, including *U. ornatrix*, use hydrocarbon-based components for their sex pheromones. We wonder whether the difference between *U. ornatrix* and *H. zea* pore positionings at the bases of the ridges versus the planar inter-ridge regions, respectively, is related to the physical chemistry of adsorption of hydrocarbons versus more polar compounds. However, the pores of at least one polar compound-utilizing species, *Bombyx mori*, appear to often reside at or near the bases of ridges (Fig. 4A; Steinbrecht, 1999). We detected no heterogeneity of the lipid coatings on the *U. ornatrix* sensilla along the ridge-crests (Fig. 11B and E), whereas there was consistently greater hydrophobicity along these crests in *H. zea* than on the inter-ridge planar areas containing the pores (Fig. 10A–D). It is intriguing to think that some kind of lipid coating gradient might guide molecules down the pores and expedite pheromone component transport into the sensillum lumen. At this point we cannot explore the pore entrances themselves with AFM/CFM imaging without encountering phase-shift artifacts seemingly caused by the sides of our current tips contacting the pore-wall sides and confounding measurements of the polarity of the substances in the pores. We should soon be able to attain greater resolution by using new, narrower AFM tips made of carbon nanotubes, and this will be among our next steps in trying to understand in greater detail the surface lipid chemical heterogeneity involved in the initial signal acquisition steps of sex pheromone olfaction.

Acknowledgments

This research was supported by grants from the Office of Naval Research (Counter-IED Program); the Defense Threat Reduction Agency; and the United States Department of Agriculture/Animal Plant Health Inspection Service (Remote Sensor Development). We thank Bryan Banks for constructing the piezo cutting device, rearing the moths, and other technical assistance.

References

Adam, G., Delbrück, M., 1968. Reduction of dimensionality in biological diffusion processes. In: Rick, A., Davidson, N. (Eds.), Structural Chemistry and Molecular Biology. Freeman, San Francisco, pp. 198–215.

Allara, D.L., Parikh, A.N., Rondelez, F., 1995. Evidence for a unique chain organization in long chain silane monolayers deposited on two widely different solid substrates. Langmuir 11, 2357–2360.

Bar, G., Thomann, Y., Brandsch, R., Cantow, H.J., Whangbo, M.H., 1997. Factors affecting the height and phase images in tapping mode atomic force microscopy. Study of phase-separated polymer blends of poly(ethene-co-styrene) and poly(2,6-dimethyl-1,4-phenylene oxide). Langmuir 13, 3807–3812.

Böröczky, K., Park, K.C., Minard, R.D., Jones, T.H., Baker, T.C., Tumlinson, J.H., 2008. Differences in cuticular lipid composition of the antennae of *Helicoverpa zea*, *Heliothis virescens*, and *Manduca sexta*. Journal of Insect Physiology 54, 1385–1391.

Brandsch, R., Bar, G., Whangbo, M.H., 1997. On the factors affecting the contrast of height and phase images in tapping mode atomic force microscopy. Langmuir 13, 6349–6353.

Chen, X., Davies, M.C., Roberts, C.J., Tendler, S.J.B., Williams, P.M., Davies, J., Dawkes, A.C., Edwards, J.C., 1998. Interpretation of tapping mode atomic force microscopy data using amplitude–phase–distance measurements. Ultramicroscopy 75, 171–181.

Garcia, R., Perez, R., 2002. Dynamic atomic force microscopy methods. Surface Science Reports 47, 197–301.

Hallem, E.A., Carlson, J.R., 2006. Coding of odors by a receptor repertoire. Cell 125, 143–160.

Haugstad, G., Jones, R.R., 1999. Mechanisms of dynamic force microscopy on polyvinyl alcohol: region-specific non-contact and intermittent contact regimes. Ultramicroscopy 76, 77–86.

Hillier, N.K., Vickers, N.J., 2007. Physiology and antennal lobe projections of olfactory receptor neurons from sexually isomorphic sensilla on male *Heliothis virescens*. Journal of Comparative Physiology A 193, 649–663.

Kanaujia, S., Kaissling, K.-E., 1985. Interactions of pheromone with moth antennae: adsorption, desorption and transport. Journal of Insect Physiology 31, 71–81.

Kaissling, K.-E., 2004. Physiology of pheromone reception in insects (an example of moths). Anir. Avrjp 6, 73–91.

Keil, T.A., 1982. Contacts of pore tubules and sensory dendrites in antennal chemosensilla of a silkmoth: demonstration of a possible pathway for olfactory molecules. Tissue & Cell 14, 451–462.

Keil, T.A., 1984. Surface coats of pore tubules and olfactory sensory dendrites of a silkmoth revealed by cationic markers. Tissue & Cell 16, 705–717.

Keil, T.A., 1987. Lectin-binding sites in olfactory sensilla of the silkmoth *Antheraea polyphemus*. Annals of the New York Academy of Science 510, 403–405.

Keil, T.A., 1997. Comparative morphology of sensillum development. International Journal of Insect Morphology and Embryology 26, 151–160.

Keil, T.A., Steinbrecht, R.A., 1987. Diffusion barriers in silkmoth sensory epithelia: application of lanthanum tracer to olfactory sensilla of *Antheraea polyphemus* and *Bombyx mori*. Tissue & Cell 19, 119–134.

Keil, T.A., Steiner, C., 1991. Morphogenesis of the antenna of the male silkmoth, *Antheraea polyphemus*. III. Development of olfactory sensilla and the properties of hair-forming cells. Tissue & Cell 23, 821–851.

Lawrence, P.A., 1966. Development and determination of hairs and bristles in the milkweed bug *Oncopeltus fasciatus* (Lygaeidae, Hemiptera). Journal of Cell Science 1, 475–498.

Lee, S., Bae, S.S., Medeiros-Ribeiro, G., Blackstock, J.J., Kim, S., Stewart, D.R., Ragan, R., 2008. Scanning tunneling microscopy of template-stripped Au surfaces and highly ordered self-assembled monolayers. Langmuir 24, 5984–5987.

Locke, M., 1965. Permeability of insect cuticle to water and lipids. Science 147, 295–298.

Loudon, C., Koehl, M.A.R., 2000. Sniffing by a silkworm moth: wing fanning enhances air penetration through and pheromone interception by antennae. Journal of Experimental Biology 203, 2977–2990.

Michel, B., Bernard, A., Bietsch, A., Delamarche, E., Geissler, M., Juncker, D., Kind, H., Renault, J.-P., Rothuizen, H., Schmid, H., Schmidt-Winkel, P., Stutz, R., Wolf, H., 2001. Printing meets lithography: soft approaches to high-resolution printing. IBM Journal of Research Development 45, 697–719.

Parikh, A.N., Allara, D.L., Azouz, I.B., Rondelez, F., 1994. An intrinsic relationship between molecular structure in self-assembled n-alkylsiloxane monolayers and deposition temperature. Journal of Physical Chemistry 98, 7577–7590.

Shorey, H.H., Hale, R.L., 1965. Mass-rearing of the larvae of nine noctuid species on a simple artificial medium. Journal of Economical Entomology 58, 522–524.

Steinbrecht, R.A., 1987. Functional morphology of pheromone-sensitive sensilla. In: Prestwich, G.D., Blomquist, G.J. (Eds.), Pheromone Biochemistry. Academic Press, Orlando, pp. 353–384.

Steinbrecht, R.A., 1992a. Experimental morphology of insect olfaction: tracer studies, X-ray microanalysis, autoradiography, and immunocytochemistry with silkmoth antenna. Microscope Research and Technology 22, 336–350.

Steinbrecht, R.A., 1992b. Stimulus transport and inactivation in insect olfactory sensilla: functional morphology, tracer experiments, and immunocytochemistry. In: Singh, R.N. (Ed.), Nervous Systems – Principles of Design and Function. Wiley Eastern, New Delhi, pp. 417–435.

Steinbrecht, R.A., 1997. Pore structures in insect olfactory sensilla: a review of data and concepts. International Journal of Insect Morphology and Embryology 26, 229–245.

Steinbrecht, R.A., 1999. Olfactory receptors. In: Eguchi, E., Tominaga, Y. (Eds.), Atlas of Arthropod Sensory Receptors – Dynamic Morphology in Relation to Function. Springer, Tokyo, pp. 155–176.

Steinbrecht, R.A., Kasang, G., 1972. Capture and conveyance of odour molecules in an insect olfactory receptor. In: Schneider, D. (Ed.), Olfaction and Taste IV. Wissenschaftliche Verlagsgesellschaft, Stuttgart, pp. 193–199.

Steinbrecht, R.A., Müller, B., 1971. On the stimulus conducting structures in insect olfactory receptors. Zeitschrift für Zellforschung and Mikroskopiscne Anatomie 117, 570–575.

Ulman, A., 1996. Formation and structure of self-assembled monolayers. Chemistry Review 96, 1533–1554.

Weiss, E.A., Kaufman, G.K., Kriebel, J.K., Li, Z., Schalek, R., Whitesides, G.M., 2007. Si/SiO_2-templated formation of ultraflat metal surfaces on glass, polymer, and solder supports: their use as substrates for self-assembled monolayers. Langmuir 23, 9686–9694.

Whitesides, G.M., Ostuni, E., Takayama, S., Jiang, X., Ingber, D.E., 2001. Soft lithography in biology and biochemistry. Annual Review of Biomedical Engineering 3, 335–373.

Zhu, Z., Daniel, T.A., Maitani, M., Cabarcos, O.M., Allara, D.L., Winograd, N., 2006. Controlling gold atom penetration through alkanethiolate self--assembled monolayers on Au{111} by adjusting terminal group intermolecular interactions. Journal of the American Chemical Society 128, 13710–13719.